AJNR

T1 and T2 measurements of meningiomas and neuromas before and after Gd-DTPA.

T Watabe and T Azuma

AJNR Am J Neuroradiol 1989, 10 (3) 463-470
http://www.ajnr.org/content/10/3/463

T1 and T2 Measurements of Meningiomas and Neuromas Before and After Gd-DTPA

Tsuneya Watabe[1]
Tomoko Azuma

Seven patients with meningiomas and five patients with neuromas were examined with spin-echo sequences on a 0.35-T imaging system. Signal enhancement and relaxation rate increments with gadolinium-diethylenetriamine pentaacetic acid (Gd-DTPA) were evaluated, as well as relaxation rate contributions, indicators of Gd-DTPA accessibility to the tissue water. The average signal enhancement rate with Gd-DTPA was higher in neuromas than in meningiomas, 148% and 84%, respectively, but this difference was poorly appreciated on enhanced images because of similar average postcontrast T1 values in both tumors. However, the average T1 relaxation increment was almost twofold higher in neuromas than in meningiomas, 318% and 162%, respectively, mainly deriving from longer intrinsic T1 values in neuromas. Also, there was a 25% increase in the average T2 relaxation rate in neuromas after Gd-DTPA together with a higher T2 contribution by Gd-DTPA, while such effects were hardly discernible in meningiomas, suggestive of greater accessibility of Gd-DTPA to the tissue water in neuromas.

By electron microscopy, endothelial fenestration and open gap junctions are commonly found in capillaries of both tumors, functioning as the routes into the extracellular space where the major contrast effect of Gd-DTPA can be expected. However, the open gap junctions are short and straight in neuromas, while they are tortuous and sinusoid in meningiomas. This may provide greater access for contrast material into relatively larger extracellular spaces in neuromas and may cause a greater T1 relaxation rate increment with Gd-DTPA. Although of limited clinical value, the different T1 and T2 relaxation rate increments with Gd-DTPA occasionally may provide useful information in the differential diagnosis, especially with mass lesions in the cerebellopontine angle and skull base.

Gd-DTPA was found to provide useful information about T1 relaxation effects in meningiomas and neuromas and may help distinguish between them.

In MR imaging, a technique sensitive to the behavior of tissue water, the signal intensity of any tissue is quite dependent on the biologic distribution of the water protons in it [1], apart from those proton signals pertinent to lipids or neutral fats. The contrast enhancement in MR imaging is based on the strong alteration of the relaxation process of the water protons in the presence of any paramagnetic agent within a certain lesion or tissue [2], and gadolinium-diethylenetriamine pentaacetic acid (Gd-DTPA) is a well-known MR contrast agent used for this effect [2, 3], particularly for the T1 relaxation effect. Many reports of its experimental and clinical efficacy in various disorders of the CNS have been published; these reports have focused mainly on processes associated with impairment of the blood-brain barrier, such as primary and metastatic brain tumors [4–8], brain abscesses [9], and ischemic [10, 11] and demyelinating foci [7], which permit leakage of the contrast material into the extracellular space where the major relaxation effect can be expected [3].

In addition to increased detectability in intracerebral lesions, increased contrast effect has also been reported in many extraaxial tumors including meningiomas and neuromas [4, 8, 12–16], but the use of Gd-DTPA for those lesions is still controversial because of the capability of conventional MR images to clearly

Received July 8, 1988; accepted after revision November 4, 1988.

[1] Both authors: Department of Radiology, Tokai University School of Medicine, Bohseidai, Isehara City, Kanagwa Pref. 259-11, Japan. Address reprint requests to T. Watabe.

AJNR **10:463–470, May/June 1989**
0195–6108/89/1003–0463

delineate them with properly chosen pulse sequences [4]. However, what is important in the use of Gd-DTPA is that it can alter the relaxation process of the water protons in any pathologic tissue, and that it may be possible to obtain information about its tissue character. A previous report concerning meningiomas and neuromas revealed a greater percentage increase of signal intensities in neuromas on T1-weighted spin-echo images after Gd-DTPA injection [16], although the pathologic basis for this finding was not established.

It is our purpose to report on the differences in T1 and T2 relaxation times in meningiomas and neuromas after Gd-DTPA enhancement in 12 patients and to discuss the mechanisms involved and the possible diagnostic significance of our findings.

Subjects and Methods

Five patients with neuromas and seven with meningiomas (four men and eight women 27–76 years old) had lesions detected by contrast-enhanced CT examinations. All patients were examined on a 0.35-T superconducting magnet system* with a head coil having a 24-cm field of view, 256 × 256 matrices corresponding to a pixel size of 0.95 × 0.95 mm, and consecutive 10-mm-thick slices. The histology of each lesion was verified by a surgically obtained specimen.

The spin-echo MR images were obtained before and after IV injection of Gd-DTPA.† The parameters chosen for imaging were 500/30/2 (TR/TE/excitations) for T1-weighted images and 2000/50,100,150/2 for T2 calculation (TE = 50 and 100 msec) and T2-weighted images (TE = 150 msec). The dose of Gd-DTPA used for each patient was 0.1 mmol/kg; the postcontrast sequences were performed 5 min after injection of contrast material: the T1-weighted sequence was first, followed by a multiecho T2-weighted sequence. The total examination time for one patient for both pre- and postcontrast images was approximately 60 min. To prepare for the subsequent calculation of the relaxation times of the lesions, and also to avoid the possibility of too wide a range of signal intensities after Gd-DTPA enhancement, the RF gain primarily adjusted to the long TR sequence was applied directly to the short TR sequence at the expense of making T1-weighted images somewhat noisier and was kept at the same level before and after enhancement.

The calculation of the relaxation times and rates was based on measurement of the mean signal intensity values of a given pathologic region of interest (ROI) on each sequence. Usually the ROI comprised more than 32 pixels, except in one case where an acoustic neuroma was mostly confined within the internal auditory canal and the size of the ROI was limited. The signal data on 2000/50 and 2000/100 images were used for T2 calculation because the intensity values on 2000/150 images occasionally suffered from wide standard deviation values due to decreased signal-to-noise ratios. Because all lesions except the small neuroma already mentioned were identified on at least three consecutive slices after enhancement, the measurement was primarily performed on the center slice of each enhanced lesion in order to reduce the effect of partial-volume averaging. Though the ROI setting was aimed at an area of relatively homogeneous intensity of measurable size on both pre- and postcontrast images, on several occasions measurements were compromised because the precontrast intensity was less homogeneous than that after Gd-DTPA enhancement.

* Diasonics, Milpitas, CA.
† Schering A/G, Berlin, W. Germany.

The signal data stored in our system were based on two 16-bit words that provided a signal-intensity range of 0–32,767 on spin-echo sequences, in which the preliminary measurement of the signal intensities of the lesions before and after Gd-DTPA injection revealed a range of 2000–8000 on 500/30 sequences and of 4300–8900 on 2000/50 sequences. The standard deviation values, usually within 5% of the mean signal intensities on 2000/50 sequences but noted to become greater and to suffer increased noise levels due to either TR shortening or TE elongation with the fixed number of excitations and RF gain, were neglected, although we were aware that this would add the problem of the effect of partial-volume averaging in the subsequent data analysis. The mathematical algorithm used for the calculation of relaxation times was based on the method proposed by Riederer et al. [17]. After injection of Gd-DTPA, the rate of signal enhancement was estimated by the difference between the postcontrast and precontrast signal intensity values divided by the latter.

For the estimation of the Gd-DTPA contribution to the relaxation times, two methods were used. One method was simple estimation of the increment values of relaxation rates (1/T1 and 1/T2) after Gd-DTPA injection in the same way as in the estimation of the signal enhancement rate. The other method was the estimation of the relaxation rate contribution by Gd-DTPA to the bulk water; this value can be provided by using the equation proposed by Gadian et al. [2]:

$$R1 = 1/T1_{post} - 1/T1_{pre} \quad (1)$$

where R1 is the T1 relaxation rate contribution by Gd-DTPA to the bulk water, $T1_{pre}$ is the intrinsic T1 relaxation time of a given tissue, and $T1_{post}$ is the corresponding relaxation time in the presence of Gd-DTPA. R2 would be the equivalent calculation with the measured T2 relaxation times. Those relaxation rate contributions depend on complex parameters including the concentration ratio of paramagnetic ion to water and the number of water molecules bound to each ion [2]; roughly, however, they are the indicators of the degree of accessibility of Gd-DTPA to the tissue water. From this equation we can observe two basic factors involved in the postcontrast relaxation rate values: (1) the original tissue condition in terms of the distribution of water protons and (2) an extrinsic effect that Gd-DTPA itself has on the tissue water. It should be noted also that the relaxation rate increment corresponds to the product of this relaxation rate contribution value and the intrinsic relaxation time.

Results

A summary of the patient data is given in Table 1. Although the meningioma lesions varied in location, four neuromas were of acoustic nerve origin, with three of them in the cerebellopontine angle and the last one chiefly confined within the internal auditory canal. Also, one facial nerve neuroma extended into the middle cranial fossa (Fig. 1). Precontrast T1-weighted images in meningioma patients showed the lesion to be isointense to slightly hypointense relative to normal brain tissue (Figs. 2 and 3), but their signal intensities became isointense or hyperintense on T2-weighted images. In neuromas, signal intensities before enhancement tended to be relatively hypointense relative to normal brain tissue on T1-weighted images (Figs. 1 and 4) but were almost uniformly hyperintense on T2-weighted images.

After Gd-DTPA injection, T1-weighted images in both patient groups demonstrated prominent contrast enhancement

TABLE 1: Histologic and Imaging Findings in Patients with Meningiomas and Neuromas

Lesion: Case No.	Age	Gender	Location	SER (%)		Relaxation Times (msec)				RRI (%)		RR	
						Precontrast		Postcontrast					
				T1WI	T2WI	T1	T2	T1	T2	T1WI	T2WI	T1	T2
Meningioma (endotheliomatous):													
1	76	M	L convexity	83	0	1046	102	297	102	252	0	2.4	0.0
2	76	F	R orbital roof	81	5	1098	114	415	103	165	11	1.5	0.9
3	42	F	R tentorium	41	3	1049	84	522	84	101	0	1.0	0
4	69	F	L intraventricular (trigone)	138	41	1472	123	564	108	161	14	1.1	1.1
5	72	F	R convexity	128	23	1435	98	411	95	249	3	1.7	0.3
Meningioma (fibroblastic):													
6	73	F	L convexity	58	−2	953	85	447	76	113	12	1.2	1.4
Meningioma (transitional):													
7	59	F	L CPA	59	7	944	86	491	80	92	8	1.0	0.9
Mean				84	11	1142	99	450	93	162	7	1.4	0.7
(SD)				(34)	(14)	(206)	(13)	(79)	(7)	(61)	(5)	(0.5)	(0.5)
Neuroma:													
8	27	M	R IAC to CPA	74[a]	−1	965	108	466	83	107	30	1.1	2.8
9	44	M	R CPA	134	6	1418	86	325	68	336	26	2.4	3.1
10	38	F	R CPA	201	50	3224	106	565	102	471	4	1.5	0.4
11	36	F	R CPA	195	22	2163	133	361	112	499	19	2.3	1.4
12	30	M	L temporal bone to middle fossa	136	−19	1119	131	406	91	176	44	1.6	2.1
Mean				148	12	1778	113	425	91	318	25	1.8	2.1
(SD)				(47)	(23)	(832)	(16)	(83)	(16)	(155)	(12)	(0.4)	(0.9)

Note.—-T1WI = T1-weighted image; T2WI = T2-weighted image; SER = signal enhancement rate; RRI = relaxation rate increment; R1 and R2 = Gd-DTPA contributions to T1 and T2 relaxation rates (per second); L = left; R = right; CPA = cerebellopontine angle; IAC = internal auditory canal.

[a] The pixel number for measurement was very limited because of the small size of the lesion on the image.

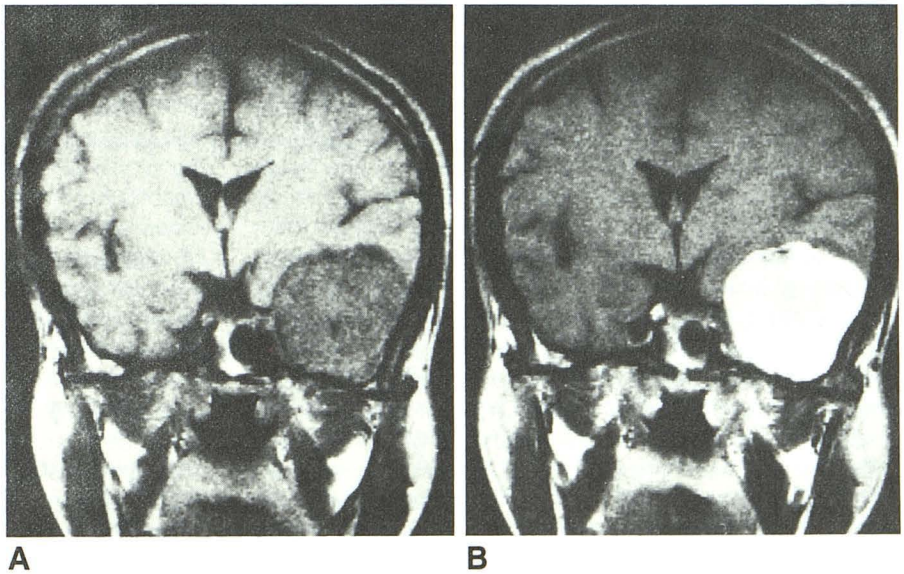

Fig. 1.—Case 12: 30-year-old man with large neuroma of facial nerve origin extending into left middle fossa.

***A*, Precontrast T1-weighted image (500/30) shows large hypointense extraaxial mass occupying left middle fossa with upward displacement of adjacent temporal lobe.**

***B*, Postcontrast T1-weighted image at same level shows remarkable enhancement of mass. Window and center levels are different from those of precontrast image (brain darker).**

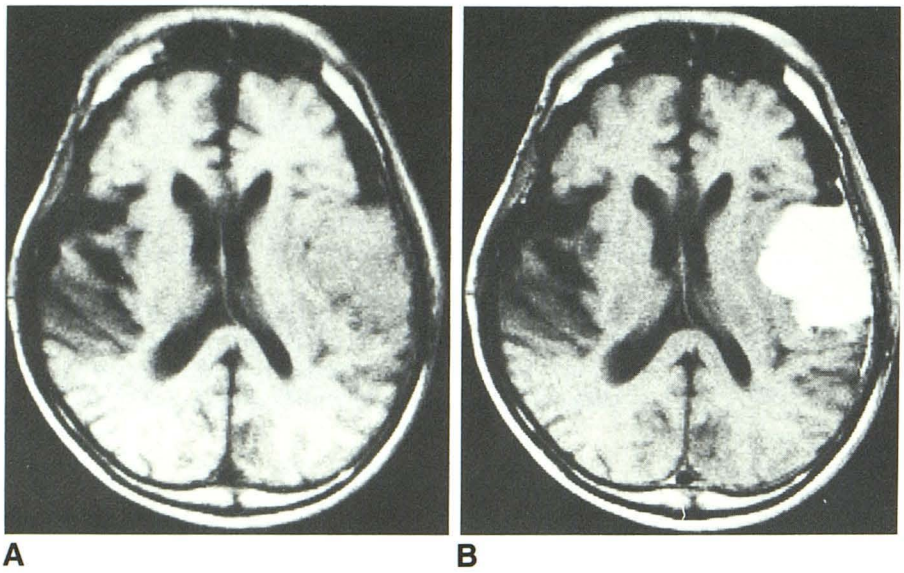

Fig. 2.—Case 1: 76-year-old man with left convexity meningioma.

A, Precontrast T1-weighted image (500/30) shows isointense to slightly hypointense extraaxial mass lesion along left convexity displacing sylvian fissure medially. Its close contact with adjacent inner table is indicative of meningioma.

B, Postcontrast T1-weighted image shows diffuse enhancement of mass with increased dural enhancement along lesion [13].

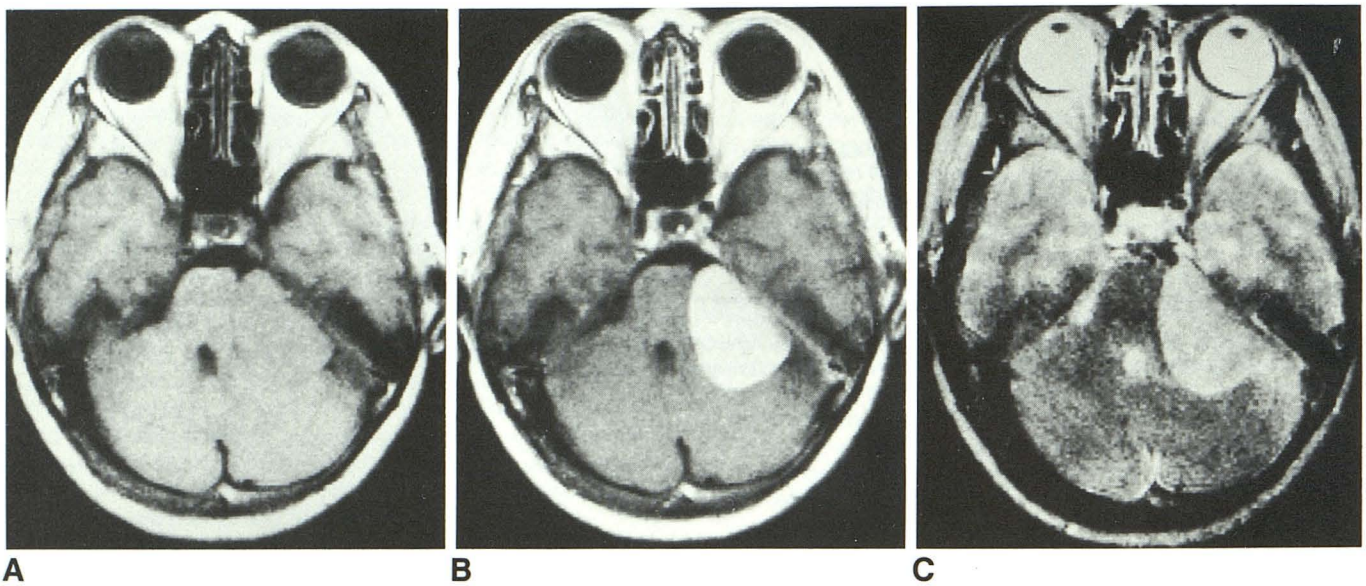

Fig. 3.—Case 7: 59-year-old woman with meningioma in left cerebellopontine angle.

A, Precontrast T1-weighted image (500/30) shows isointense mass in left cerebellopontine angle displacing brainstem and fourth ventricle medially.

B, Postcontrast T1-weighted image shows enhancement of lesion.

C, Postcontrast T2-weighted image (2000/150) delineates lesion as structure of high intensity, though signal pattern on precontrast T2-weighted image (not shown) was about the same.

of the lesions (Figs. 1–4), but there were no remarkable differences in the degrees of signal brightness on visual assessment. On T2-weighted images the signal intensities of the lesions remained grossly the same before and after enhancement. The diagnosis of those lesions on MR images was based mainly on their location, type of extension, and precontrast signal intensities on T1- and T2-weighted images rather than on their enhanced signal patterns, together with a secondary change such as prolonged dural enhancement along the lesion in meningiomas (Fig. 2) [13]. The precontrast T1-weighted images of one patient with an acoustic neuroma revealed a cystic component to the lesion that was not seen on T2-weighted images, but the interface between the cystic and solid parts was delineated more clearly on postcontrast T1-weighted images (Fig. 4). In no case was there too wide a range of signal values after Gd-DTPA injection.

On both pre- and postcontrast T1-weighted images, the average signal enhancement rate was 84 ± 34% (mean ± SD) in meningiomas and 148 ± 47% in neuromas (Table 1), although this numeric difference could not be appreciated well

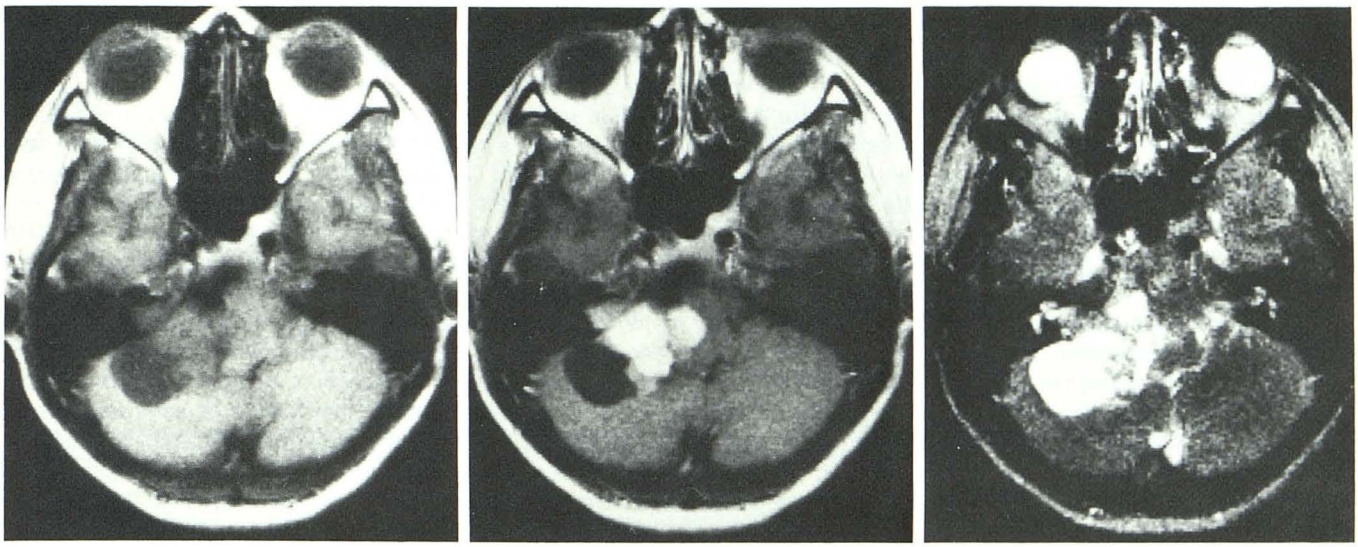

Fig. 4.—Case 11: 36-year-old woman with acoustic neuroma extending into right cerebellopontine angle.

***A*, Precontrast T1-weighted image (500/30) shows relatively hypointense mass in right cerebellopontine angle displacing brainstem and fourth ventricle medially, with extension into right internal auditory canal. Large cyst is present posteriorly.**

***B*, Postcontrast T1-weighted image shows remarkable enhancement of solid part of lesion, including its intrameatal part, a key finding in diagnosis; interface between cystic and solid parts becomes more distinctive. Note that window and center levels are different from those on precontrast image.**

***C*, Postcontrast T2-weighted image (2000/150) delineates whole lesion as structure of high intensity, and interface between cystic and solid parts becomes quite indistinct. This pattern was grossly the same on precontrast T2-weighted image (not shown).**

on the images (Figs. 1–4). The precontrast T1 relaxation times in neuromas tended to be longer than those in meningiomas, with mean values of 1778 ± 832 msec and 1142 ± 206 msec, respectively. However, the same relaxation times after Gd-DTPA shortened to almost the same value: an average of 425 ± 83 msec in neuromas and 450 ± 79 msec in meningiomas, both of which are shorter than the given TR (500 msec) set for T1-weighted images. Also, the standard deviation of T1 relaxation times in neuromas, ranging widely before Gd-DTPA injection, was about the same as that of meningiomas after enhancement.

There was a great difference in T1 relaxation rate increment values between meningiomas and neuromas, permitting a rather wide range in the standard deviation values: 162 ± 61% and 318 ± 155%, respectively, showing an almost twofold higher average increment in the latter (Table 1). The mean T2 relaxation time in neuromas was relatively longer than that in meningiomas before enhancement but became shortened after enhancement, to the same range as in meningiomas, resulting in an approximately 25% increase in the T2 relaxation rate increment on average. The mean values of the T1 relaxation rate contributions (per second) with Gd-DTPA were 1.4 ± 0.5 in meningiomas and 1.8 ± 0.4 in neuromas, indicating a less significant difference in both tumor groups, as compared with the difference in T1 relaxation rate increments. However, the average T2 contribution value in neuromas was more than twofold higher than that in meningiomas, although this effect was not remarkable on the visual assessment.

Discussion

The rather wide range of measurements, which led to a large standard deviation for each calculated value, was a problem in analyzing our data. Because all tumors except one small neuroma were sizable and were identified on at least three consecutive slices, we assumed that we could reduce the volume-averaging effect by focusing the ROI on any homogeneously enhanced part near the center of the lesion. However, this led us on several occasions to perform compromised measurements on a part with less homogeneous intensity on the corresponding precontrast image. In addition, another volume-averaging effect, deriving from rather variable signal-to-noise ratios among sequences with a fixed number of excitations and RF gain, must be considered. Also, the tissue condition of each lesion, which affects the degree of signal enhancement, appeared to have been somewhat inconsistent, even in the same tumor group. These factors were believed to be the major reasons for the variability in measurements and affected our ability to analyze our data.

Using a 1.5-T imaging system, Breger et al. [16] reported 180% and 310% increases in average signal intensity values with Gd-DTPA on T1-weighted spin-echo images of eight meningioma lesions and nine neuroma lesions, respectively, and inferred that more than a 300% increase in the signal intensity value after enhancement would more likely reflect a neuroma than a meningioma [16]. In our data, the average signal enhancement rate of neuromas on T1-weighted images was 148% and was 64% higher than that of meningiomas,

basically consistent with the result of Breger et al., apart from the obtained numeric values, which could be related to the strength of the static magnetic field. However, this difference was not appreciated on visual assessment, because, unlike CT, MR images have no determined scale factor with respect to the signal intensity, and the adjustment of window and center levels to a given area or lesion tends to be dependent on either the operator or the signal brightness (Figs. 1 and 4), making such a contrast effect from Gd-DTPA somewhat nonspecific.

The unremarkable difference between postcontrast T1 relaxation times in meningiomas and neuromas, 450 and 425 msec on average, all shorter than the TR (500 msec) set for the T1-weighted sequence, makes the tumors similar after enhancement. Similar results have been reported at 0.15 T with similar pulse sequences [12, 14]. Allowing for some estimation errors due to the limited data in these reports, the average T1 relaxation times after enhancement were approximately 360 msec in meningiomas and 383 msec in neuromas, all shorter than the inversion time (TI = 500 msec) of the inversion-recovery sequence used. These facts suggest that evaluation of the signal pattern of the enhanced image alone may be invalid.

What was more significantly different between meningiomas and neuromas in our data was the almost twofold higher average T1 relaxation rate increment in neuromas (Table 1). Our calculations, based on the data in the above reports [12, 14], revealed that the average T1 relaxation rate increments were approximately 100% in neuromas and 55% in meningiomas. Because our data reflect the distribution of the water protons in certain tissue and the accessibility of Gd-DTPA to that tissue, it can be inferred that this difference in T1 relaxation rate increments may be related to the tissue characteristics of each tumor group.

Gd-DTPA is known to first react with water protons bound to it, usually a small fraction of the tissue water. The fast exchange with those protons in the bulk water causes a great relaxation effect on them and hence on the pathologic tissue containing them [2]. This implies that on T1-weighted images, the signal intensity of any Gd-DTPA–enhanced lesion is usually higher than that of other structures or tissues; this is not a simple reflection of the local Gd-DTPA concentration in it, but is the dual effect of both its intrinsic T1 relaxation time and T1 relaxation rate contribution, as indicated in equation 1. Our results tell us that this dual effect was significantly greater in neuromas than in meningiomas, mainly due to the relatively longer T1 relaxation times in neuromas, as shown by our data (Table 1) and by those of others [15].

Although the difference in T1 relaxation rate contributions with Gd-DTPA was unremarkable in both tumor groups, there was a moderately higher average T2 contribution in neuromas. Because the relaxation rate contribution by Gd-DTPA is complex [2], any conclusion based on this result should be guarded. However, it may be said, that the 25% increase in the average T2 relaxation rate in neuromas may indicate that Gd-DTPA is more accessible to the tissue water protons in neuromas to the extent that it can cause a certain degree of T2 shortening effect in the lesions. The same T2 shortening effect by Gd-DTPA in neuromas (33% decrease) was reported by Curati et al. [14].

It is well known that both meningiomas and neuromas can demonstrate a considerable degree of enhancement on contrast-enhanced CT images [18]; this enhancement usually is more prominent in meningiomas, partly reflecting their rich vascularity, as frequently shown by angiography. Gd-DTPA has a molecular weight similar to that of the iodinated contrast material used in CT, and it uses grossly the same mechanism for its access route to tissues [3, 4]. The accumulation of contrast material is dependent on two factors [19]. One factor is the inherent tumor vascularity or macroscopic vascular flow to a lesion; this regulates the volume of contrast material washed in and out with subsequent balancing of the contrast levels. The other factor is the predominantly extracellular accumulation of these contrast agents [3, 19]. This plays an important role in the mechanism of Gd-DTPA enhancement, as inferred by the fact that such an accumulation of the contrast substances in the extracellular space can be suppressed by increasing the molecular weight of the contrast agent, such as by using Gd-DTPA labeled with albumin [20]. With respect to this point, both tumors show similar capillary endothelial structures at the electron microscopic levels [21–23]. However, our results, which show different T1 and T2 relaxation rate increments in meningiomas and neuromas, raise a question about what is different in their tissue environments in terms of the accessibility of Gd-DTPA to the tissue water.

Hirano et al. [21] first reported the presence of numerous fenestrae in the blood vessels of neurilemomas on electron microscopic observation and inferred that these fenestrae were responsible for the massive exchange of fluid between the circulatory system and parenchyma and could be a factor in the formation of cystic spaces, which were not uncommon in this tumor [21]. According to Hirano et al., the capillary structures can be divided into two types on the basis of the presence or absence of fenestrae, and the blood vessels in the nervous tissue provide the best example of their absence. The fenestrated membranes are small islands of endothelium connected by individual single membranes and tend to rupture, making large gaps in vascular walls (Fig. 5A) from which such a heavy molecule as protein can pass into the extracellular space [22]. This fenestration has been found in many human tumors, including hemangiopericytoma [24], choroid plexus papilloma [25], primary melanoma of the CNS [26], metastatic renal cell carcinoma [27], and pituitary adenoma [28]. It is also found in both meningiomas and neuromas, though more commonly in meningiomas [22, 23]. Another communicating space between the capillary lumen and the extracellular space is the gap junction between endothelial cells. A type of tight gap junction is known to function as a blood-brain barrier [29]. However, the tight gap junction is absent in extramedullary tumors, and Long [22] found instead an open gap junction analogous to it in meningiomas and neuromas, though such a barrier function is absent.

Both the fenestration and the open gap junction function

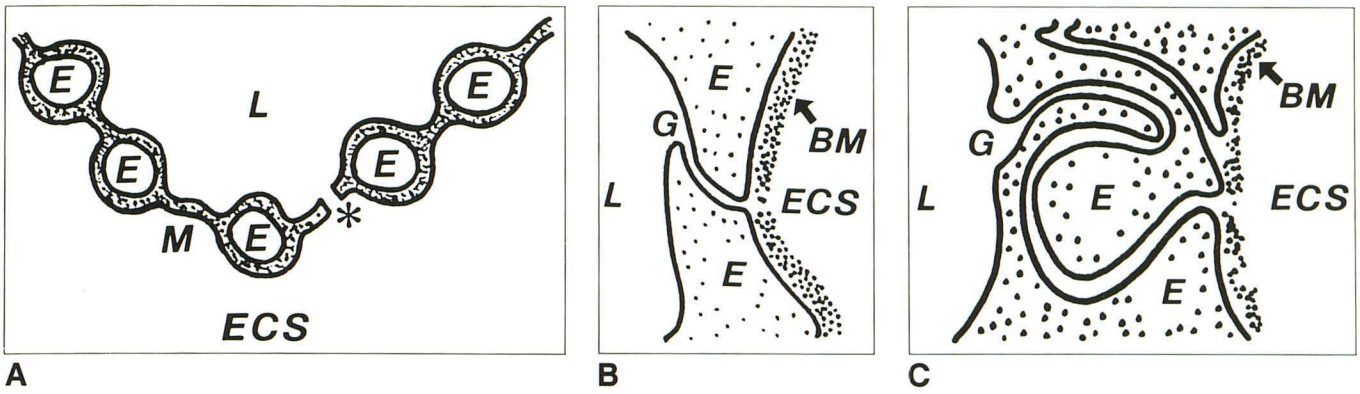

Fig. 5.—Schematic representation of endothelial fenestrae and gap junctions in neuromas and meningiomas [21–23].

***A*, Endothelial fenestrae are small islands of endothelium (E) connected by single membranes (M) that occasionally may rupture (*asterisk*) and allow free communication between capillary lumen (L) and extracellular space (ECS).**

***B*, Open gap junction (G) in neuroma has short and straight course, and communication between capillary lumen (L) and extracellular space (ECS) through it is patent. Also, ECS is usually wide in neuroma and basement membrane (BM) is well defined.**

***C*, Open gap junction (G) in meningioma is tortuous and sinusoid with less regular lining of basement membrane (BM). Endothelial cells (E) along sinusoid often are similar to tumor cells. This sinusoidal pattern makes route to extracellular space (ECS) longer and redundant.**

as nutritional pathways from the vascular lumen to the extracellular space in those tumors [22] and hence as the major routes of the contrast material into the same space. However, the capillary structures in neuromas are much simpler and the gap junctions in them are usually short, straight, and patent [23], freely communicating with a relatively large extracellular space (Fig. 5B) [22]. In meningiomas, the gap junctions are often tortuous, elongated, sinusoid, and frequently lined by abnormal endothelial cells similar to tumor cells (Fig. 5C). This situation may limit accumulation of the contrast material in the extracellular space to some extent, although straighter open gap junctions are also found in capillaries of relatively large size.

The diagnosis of meningiomas and neuromas usually is easy in clinical imaging studies. However, it may be difficult to make the diagnosis with CT and MR if the lesions are in the cerebellopontine angle or in the skull base. Although there was a rather premature conclusion that both tumors have distinctly different intensity features on precontrast T2-weighted images [13], it has been found that this is not always accurate [30, 31], even when Gd-DTPA is used. Our results, though limited, indicate that in such cases Gd-DTPA may yield useful information about different T1 relaxation effects in each tumor group, and allow preoperative differentiation between the two. The clinical value is apt to be limited, but we believe our data in meningiomas and neuromas with Gd-DTPA will encourage further investigation of other extraaxial tumors in terms of their tissue characterization.

REFERENCES

1. Mansfield P, Pykett IL. Biological and medical imaging by NMR. *J Magn Reson* **1978**;29:355–373
2. Gadian DG, Payne JA, Bryant DJ, Young IR, Carr DH, Bydder GM. Gadolinium-DTPA as a contrast agent in MR imaging—theoretical projections and practical observations. *J Comput Assist Tomogr* **1985**;9:242–251
3. Weinmann HJ, Brasch RC, Press WR, Wesbey GE. Characteristics of Gadolinium-DTPA complex: a potential NMR contrast agent. *AJR* **1984**;142:619–624
4. Felix R, Shorner W, Laniado M, et al. Brain tumours: MR imaging with gadolinium-DTPA. *Radiology* **1985**;156:681–688
5. Claussen C, Laniado M, Schörner W, et al. Gadolinium-DTPA in MR imaging of glioblastomas and intracranial metastases. *AJNR* **1985**;6:669–674
6. Graif M, Bydder GM, Steiner RE, Niendorf P, Thomas DGT, Young IR. Contrast-enhanced MR imaging of malignant brain tumors. *AJNR* **1985**;6:855–862
7. Brant-Zawadzki M, Berry I, Osaki L, Brasch R, Murovic J, Norman D. Gd-DTPA in clinical MR of the brain: 1. Intraaxial lesions. *AJNR* **1986**;7:781–788, *AJR* **1986**;147:1223–1230
8. Stack JP, Antoun NM, Jenkins JPR, Metcalfe R, Isherwood I. Gadolinium-DTPA as a contrast agent in magnetic resonance imaging of the brain. *Neuroradiology* **1988**;30:145–154
9. Runge VM, Clanton JA, Price AC, et al. Evaluation of contrast enhanced MR imaging in a brain-abscess model. *AJNR* **1985**;6:139–147
10. McNamara MT, Brant-Zawadzki M, Berry I, et al. Acute experimental cerebral ischemia: MR enhancement using Gd-DTPA. *Radiology* **1986**;158:701–705
11. Imakita S, Nishimura T, Naito H, et al. Magnetic resonance imaging of human cerebral infarction: enhancement with Gd-DTPA. *Neuroradiology* **1987**;29:422–429
12. Bydder GM, Kingsley DPE, Brown J, Niendorf HP, Young IR. MR imaging of meningiomas including studies with and without gadolinium-DTPA. *J Comput Assist Tomogr* **1985**;9:690–697
13. Berry I, Brant-Zawadzki M, Osaki L, Brasch R, Murovic J, Newton TH. Gd-DTPA in clinical MR of the brain: 2. Extraaxial lesions and normal structures. *AJNR* **1986**;7:789–793, *AJR* **1986**;147:1231–1235
14. Curati WL, Graif M, Kingsley DPE, Niendorf HP, Young IR. Acoustic neuromas: Gd-DTPA enhancement in MR imaging. *Radiology* **1986**;158:447–451
15. Curati WL, Graif M, Kingsley DPE, King T, Scholtz CL, Steiner RE. MRI in acoustic neuroma: a review of 35 patients. *Neuroradiology* **1986**;28:208–214
16. Breger RK, Papke RA, Pojunas KW, Haughton VM, Williams AL, Daniels DL. Benign extraaxial tumours: contrast enhancement with Gd-DTPA. *Radiology* **1987**;163:427–429
17. Riederer SJ, Bobman SA, Lee JN, Farzaneh F, Wang HZ. Improved

precision in calculated T1 MR images using multiple spin-echo acquisition. *J Comput Assist Tomogr* **1986**;10:103–110
18. Naidich TP, Lin JP, Leeds NE, et al. Computed tomography in the diagnosis of extra-axial posterior fossa masses. *Radiology* **1976**;120:333–339
19. Som PM, Lanzieri CF, Sacher M, Lawson W, Biller HF. Extracranial tumour vascularity: determination by dynamic CT scanning. Part I: Concepts and signature curves. *Radiology* **1985**;154:401–405
20. Schmiedl U, Ogan M, Paajanen H, et al. Albumin labeled with Gd-DTPA as an intravascular, blood pool-enhancing agent for MR imaging: biodistribution and imaging studies. *Radiology* **1987**;162:205–210
21. Hirano A, Dembitzer HM, Zimmerman HM. Fenestrated blood vessels in neurilemoma. *Lab Invest* **1972**;27:305–309
22. Long DM. Vascular ultrastructure in human meningiomas and schwannomas. *J Neurosurg* **1973**;38:409–419
23. Kasantikul V, Glick AD, Netsky MG. Light and electron microscopic observations of blood vessels in neurilemoma. *Arch Pathol Lab Med* **1979**; 103:683–687
24. Ramsey HJ. Fine structure of hemangiopericytoma and hemangio-endothelioma. *Cancer* **1966**;19:2005–2018
25. Carter LP, Beggs J, Waggener JD. Ultrastructure of three choroid plexus papillomas. *Cancer* **1972**;30:1130–1136
26. Ward JD, Hadfield MG, Becker DP, Lovings ET. Endothelial fenestration and other vascular alterations in primary melanoma of the central nervous system. *Cancer* **1974**;34:1982–1991
27. Hirano A, Zimmerman HM. Fenestrated blood vessels in a metastatic renal carcinoma in the brain. *Lab Invest* **1972**;26:465–468
28. Schelin U. Chromophobe and acidophil adenomas of the human pituitary gland. A light and electron microscopic study. *Acta Pathol Microbiol Immunol Scand [Suppl]* **1962**;158:5–80
29. Brightman MW, Klatzo I, Olsson Y, Reese TS. The blood-brain barrier to proteins under normal and pathological conditions. *J Neurol Sci* **1970**; 10:215–239
30. Mikhael MA, Ciric IS, Wolff AP. Differentiation of cerebellopontine angle neuromas and meningiomas with MR imaging. *J Comput Assist Tomogr* **1985**;9:852–856
31. Press GA, Hesselink JR. MR imaging of cerebellopontine angle and internal auditory canal lesions at 1.5 T. *AJNR* **1988**;9:241–251, *AJR* **1988**; 150:1371–1381